BIOCHEMISTRY
including biophysical chemistry & molecular biology

Article

pubs.acs.org/biochemistry

Investigation of the Inhibitory Effect of Nitrite on Photosystem II

Ravi Pokhrel and Gary W. Brudvig*

Department of Chemistry, Yale University, New Haven, Connecticut 06520-8107, United States

Supporting Information

ABSTRACT: The role of chloride in photosystem II (PSII) is unclear. Several monovalent anions compete for the Cl^- site(s) in PSII, and some even support activity. NO_2^- has been reported to be an activator in Cl^--depleted PSII membranes. In this paper, we report a detailed investigation of the chemistry of NO_2^- with PSII. NO_2^- is shown to inhibit PSII activity, and the effects on the donor side as well as the acceptor side are characterized using steady-state O_2-evolution assays, electron paramagnetic resonance (EPR) spectroscopy, electron-transfer assays, and flash-induced polarographic O_2 yield measurements. Enzyme kinetics analysis shows multiple sites of NO_2^- inhibition in PSII with significant inhibition of oxygen evolution at <5 mM NO_2^-. By EPR spectroscopy, the yield of the S_2 state remains unchanged up to 15 mM NO_2^-. However, the S_2-state $g = 4.1$ signal is favored over the $g = 2$ multiline signal with increasing NO_2^- concentrations. This could indicate competition of NO_2^- for the Cl^- site at higher NO_2^- concentrations. In addition to the donor-side chemistry, there is clear evidence of an acceptor-side effect of NO_2^-. The $g = 1.9$ Fe(II)-$Q_A^{-\bullet}$ signal is replaced by a broad $g = 1.6$ signal in the presence of NO_2^-. Additionally, a $g = 1.8$ Fe(II)-$Q^{-\bullet}$ signal is present in the dark, indicating the formation of a NO_2^--bound Fe(II)-$Q_B^{-\bullet}$ species in the dark. Electron-transfer assays suggest that the inhibitory effect of NO_2^- on the activity of PSII is largely due to the donor-side chemistry of NO_2^-. UV−visible spectroscopy and flash-induced polarographic O_2 yield measurements indicate that NO_2^- is oxidized by the oxygen-evolving complex in the higher S states, contributing to the donor-side inhibition by NO_2^-.

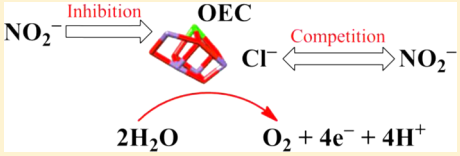

Photosystem II (PSII) is a multisubunit pigment−protein complex that catalyzes the challenging light-driven oxidation of water in oxygenic photosynthetic organisms. The active site for water oxidation, the oxygen-evolving complex (OEC), is a Mn_4CaO_5 cluster buried in the protein but with substantial access to water and other small molecules.[1,2] The metal ions in the Mn_4CaO_5 cluster are ligated by six carboxylate residues, mostly as bridging ligands, and one histidine residue.[1] In addition to the amino acid residues, four waters are also coordinated to the metals in the OEC.[1] Two of the coordinated waters, one on Mn and one on Ca, are putative substrate water molecules, according to the nucleophilic attack mechanism for O−O bond formation in the OEC.[2] PSII conducts the multielectron oxidation steps with a minimal overpotential, allowing favorable kinetics for water oxidation.

During turnover, the OEC progresses through a series of oxidation states, known as storage states or S states.[3] The most reduced state, the S_0 state, is sequentially oxidized to the most oxidized S_4 state. When an exciton, generated by photon absorption, reaches the reaction center pigments of PSII (P_{680}), they are photoexcited and initiate electron-transfer events that result in an ultrafast charge separation across the membrane bilayer, providing redox energy to oxidize the OEC. A stable charge separation is achieved between the $P680^{+\bullet}$ radical and a membrane-bound $Q_A^{-\bullet}$ semiquinone radical. The OEC is then oxidized by $P_{680}^{+\bullet}$ via a redox-active tyrosine residue, Y_Z, and $Q_A^{-\bullet}$ transfers the electron to the terminal electron acceptor in PSII, Q_B, another plastoquinone molecule. A non-heme ferrous ion lies between Q_A and Q_B. The non-heme Fe(II) is ligated by four histidine residues and one bicarbonate/carbonate ligand under physiological conditions and is not redox-active during the normal electron-transfer processes.[4−7] However, substitution of the bicarbonate/carbonate ligand with other small molecules influences the electron-transfer kinetics between Q_A and Q_B.[4,8] The OEC and the cofactors involved in electron transfer can be divided into the "donor side" and the "acceptor side" of PSII. The electron donor side consists of the cofactors that reduce $P_{680}^{+\bullet}$, including the OEC and Y_Z. The electron acceptor side consists of the cofactors involved in the transfer of an electron from P_{680} to Q_B.

It has long been known that Cl^- is essential for the maximal O_2 evolving activity in PSII,[9,10] with a stoichiometry of one high-affinity Cl^- ion per PSII determined by analyzing $^{36}Cl^-$-labeled PSII.[11] Recently, the locations of two Cl^- ions near the OEC have been identified by X-ray crystallography, and both sites are approximately 6−7 Å from the OEC.[1,12−14] Earlier EXAFS data also suggested a similar distance of Cl^- from the OEC.[15]

The role of Cl^- in PSII has been investigated by substituting different monovalent anions and studying the effects on the activity and S-state transitions of the OEC. Several monovalent anions such as Br^-, NO_3^-, I^-, CH_3COO^-, and N_3^- have been shown to compete for the Cl^--binding site.[16−18] O_2-evolution activity in Cl^--depleted PSII has been recovered in varying efficiency: $Cl^- > Br^- \gg NO_3^- > NO_2^- > I^-$.[16] Br^- substitutes almost identically for Cl^-, whereas I^- is activating at low

Received: February 17, 2013
Revised: April 30, 2013
Published: April 30, 2013

   dx.doi.org/10.1021/bi400206q | *Biochemistry* 2013, 52, 3781−3789

concentrations and becomes inhibitory at higher concentrations, possibly by reducing the OEC.[16,19] The rate of O_2 evolution restored by NO_3^- is almost as high as that in the presence of Cl^- when measured under limited light conditions.[20] Hence, NO_3^--substituted PSII is fully active for O_2 evolution, although with a slower turnover rate.[20] It has been shown that NO_3^- specifically slows the $S_3 \rightarrow S_0$ transition.[21]

Although nitrite (NO_2^-) has been reported to be activating in Cl^--depleted PSII,[16] competition of NO_2^- for the Cl^- site had not yet been studied. In addition to partial activation of Cl^--depleted PSII by NO_2^-,[16] there is evidence that NO_2^- inhibits PSII function.[22,23] Thermoluminescence investigations in spinach thylakoids with or without exogenous Cl^- added during the preparation indicate that NO_2^- interacts with the OEC, potentially modifying the S_2 state.[24] Furthermore, using flash-induced UV absorbance difference spectroscopy, it has been shown that NO_2^- may reduce the higher oxidation states of the OEC.[16] In this paper, we discuss the competition of NO_2^- with Cl^- as well as the inhibitory effects of NO_2^- as characterized by steady-state O_2-evolution assays, EPR spectroscopy, UV−visible electron-transfer assays, and flash-induced polarographic O_2 measurements.

MATERIALS AND METHODS

Steady-State Oxygen-Evolution Measurements. PSII-enriched membranes were isolated from fresh market spinach according to the procedure developed by Berthold, Babcock, and Yocum.[25] O_2 evolution was monitored using a Clark-type electrode, and the O_2 assay chamber was maintained at 25 °C. Samples were illuminated by an Oriel 1000 W tungsten halogen lamp fitted with a water filter and a 610 nm long-pass cutoff filter; 250 μM 2,5-DCBQ and 1 mM K_3FeCN_6 were used as electron acceptors during the assays. All O_2 assay buffers were prepared with 10 mM Ca^{2+} (using $CaOH_2$) and 60 mM MES. Varying concentrations of Cl^- and NO_2^- were added from NaCl and $NaNO_2$ stock solutions, respectively. Each solution was adjusted to pH 6.0 after the addition of NaCl and $NaNO_2$. O_2 assays were performed with a sample of ∼10 μg of Chl from untreated, O_2-evolving PSII membranes. Typical O_2-evolution activities of PSII membranes without any treatment were 400−530 μmol of O_2 (mg of Chl)$^{-1}$ h^{-1}.

Electron Paramagnetic Resonance Spectroscopy. EPR samples were prepared by suspending untreated, O_2-evolving PSII membranes in 10 mM Ca^{2+}, 10 mM NaCl, 25% (v/v) glycerol, and 60 mM MES-NaOH (pH 6.0) with 0, 10, 15, 30, or 60 mM $NaNO_2$. EPR scans were acquired on a Bruker ELEXSYS E500 EPR spectrometer equipped with a SHQ resonator and an Oxford ESR-900 helium-flow cryostat. The S_1-state spectra were obtained in the dark using dark-adapted PSII membranes. The S_2-state spectra were obtained after illumination of the samples in a 200 K dry ice/acetone bath for 5 min. The $S_1Y_Z^\bullet$ signal was obtained by illuminating dark-adapted PSII samples in the cryostat at 7 K. EPR scans probing the intensities of the S_2-state $g = 2$ multiline and $g = 4.1$ signals and the $S_1Y_Z^\bullet$ signal were taken at 7 K with the following instrumental parameters: microwave frequency of 9.38 GHz, modulation frequency of 100 kHz, modulation amplitude of 31 G, and microwave power of 5 mW. Some EPR scans probing the Fe(II)-$Q^{-\bullet}$ signals were taken at 4 K with the following instrumental parameters: microwave frequency of 9.38 GHz, modulation frequency of 100 kHz, modulation amplitude of 31 G, and microwave power of 20 mW.

Electron-Transfer Assays. Electron-transfer assays were performed on Mn-depleted, extrinsic polypeptide-depleted PSII membranes and on untreated, O_2-evolving PSII membranes. The extrinsic polypeptide depletion procedure and the Mn depletion procedures have been previously published.[26,27] Complete loss of O_2-evolution activity was confirmed by a Clark electrode assay. For both Mn-depleted, extrinsic polypeptide-depleted PSII membranes and O_2-evolving PSII membranes, the rates of 2,6-dichlorophenolindophenol (DCPIP) reduction on the acceptor side were assayed by following the absorbance at 600 nm, the λ_{max} for DCPIP, upon illumination of the sample using a 150 W halogen lamp. For Mn-depleted PSII membranes, 7.5 μg of Chl/mL of PSII membranes, 1 mM diphenylcarbazide (DPC), and 35 μM DCPIP were assayed in a buffer solution containing 10 mM Ca^{2+}, 40 mM NaCl, and 60 mM MES-NaOH (pH 6.0) with either 0, 2.5, 5, 15, or 30 mM $NaNO_2$ present. DPC was absent for O_2-evolving PSII membranes, and otherwise identical conditions were used. The rate of change in absorbance at 600 nm is directly proportional to the rate of electron transfer on the acceptor side of PSII in Mn-depleted PSII membranes.

Flash-Induced Oxygen Yield Measurements. Flash-induced polarographic measurements were taken using a bare platinum electrode. The electrochemical cell was comprised of a Pt disk working electrode and a Ag ring counter electrode. The Ag ring was also used as the reference electrode. PSII membranes were homogenized and preflashed 10 times at a frequency of 1 Hz using a xenon flash lamp (#FX 249, EG&G electro-optics) triggered by a FY-712 "Lite-Pac" module (EG&G electro-optics) and a BK precision 3300 pulse generator. The preflashed membranes were incubated in the dark for 30 min. For each run, dark-incubated PSII membranes (15 μg of Chl) were pipetted onto the electrode with a buffer solution containing 10 mM Ca^{2+}, 40 mM NaCl, and 60 mM MES-NaOH (pH 6.0), and the electrode was centrifuged at 4000 rpm for 10 min in a HS-4 swinging bucket rotor. Once the membranes had been pelleted, additional buffer was added with electron acceptors [250 μM DCBQ and 1 mM $K_3Fe(CN)_6$] and appropriate volumes of a 1 M $NaNO_2$ stock solution to reach the desired NO_2^- concentration (0, 2.5, 5, 15, or 30 mM). The electrode was polarized for 90 s before data were acquired, after which the flash sequence (20 flashes at 1 Hz) was initiated. The S-state parameters, misses and double hits, were obtained by fitting the data assuming a four-state Kok model.

RESULTS AND DISCUSSION

Steady-State O_2-Evolution Assays. Clark electrode-based O_2-evolution measurements of NO_2^--treated PSII samples showed a decrease in the initial rate of O_2 evolution and a rapid, progressive inhibition during steady-state turnover (Figure 1). Inhibition due to NO_2^- under steady-state illumination occurred after very short periods of dark incubation (2 min) and remained constant over the course dark incubation for 3 h (Figure S1 of the Supporting Information). Almost complete recovery of activity was observed when a PSII sample incubated in 2.5 mM NO_2^- for 3 h in the dark was washed with NO_2^--free buffer and assayed for activity (Figure S1 of the Supporting Information). This indicated reversible inhibition by NO_2^- in the dark. Hence, the inhibitory aspect of NO_2^- as seen in the steady-state O_2-evolution measurements was enhanced during turnover.

dx.doi.org/10.1021/bi400206q | Biochemistry 2013, 52, 3781−3789

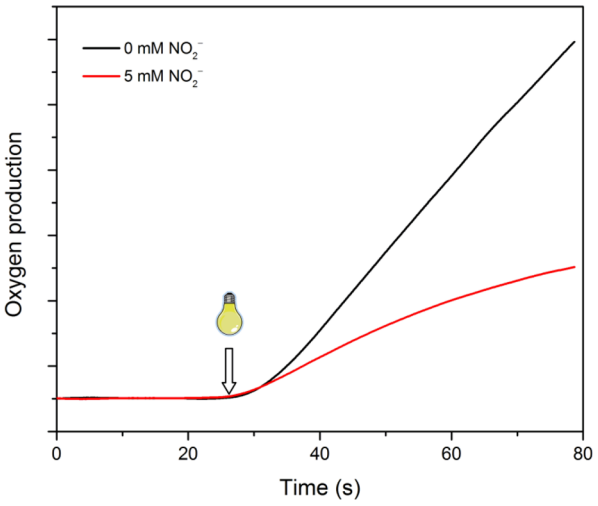

Figure 1. Characteristic O_2-evolution traces for PSII membranes assayed in the presence of 0 and 5 mM NO_2^-. Both assay buffers also contained 40 mM Cl^-, 10 mM Ca^{2+}, and 60 mM MES-NaOH (pH 6.0). DCBQ and K_3FeCN_6 were used as electron acceptors.

DCPIP Electron-Transfer Assays. DCPIP reduction assays were performed to determine if the inhibition of PSII by NO_2^-, as observed in steady-state O_2 assays, resulted from slow electron-transfer kinetics on the acceptor side or from an effect on the donor side. DCPIP reduction studies were conducted with Mn-depleted, extrinsic polypeptide-depleted, and O_2-evolving PSII membranes. For Mn-depleted PSII membranes, electron-transfer assays were conducted using DCPIP as an electron acceptor and DPC as an electron donor. For O_2-evolving PSII membranes, electron-transfer assays were conducted using DCPIP as an electron acceptor but in the absence of DPC. Therefore, any reduction of DCPIP on the acceptor side was coupled to turnover at the OEC on the donor side.

From the electron-transfer kinetics of Mn-depleted PSII membranes, it was clear that the presence of NO_2^- did not significantly slow the reduction of DCPIP on the acceptor side, although there was a slight decrease in the rate of DCPIP reduction with increasing NO_2^- concentrations (Figure 2A). In contrast, the rate of DCPIP reduction was significantly slowed with increasing concentrations of NO_2^- when the same assay was performed with oxygen-evolving PSII membranes (Figure 2B and Figure S3 of the Supporting Information): the initial rate of DCPIP reduction decreased with increasing concentrations of NO_2^- (Figure S3 of the Supporting Information), and the rate of DCPIP reduction reached a plateau much more quickly in the presence of increasing concentrations of NO_2^- (Figure 2B). These results are in agreement with the steady-state O_2-evolution measurements (Figure 1). Therefore, it is clear that the primary inhibitory effect of NO_2^- is on the donor side of PSII.

To characterize the reactions of NO_2^- with PSII, UV−visible spectra of O_2-evolving PSII membranes without NO_2^- or with 5 mM NO_2^- were obtained in the dark and after illumination for 60 s (Figure S4A of the Supporting Information). The dark-minus-light difference spectra of the two samples showed the characteristic spectrum of DCPIP between 450 and 800 nm. In addition, a change in the difference spectrum in the 300−400 nm range was observed (Figure S4B of the Supporting Information). A double-difference spectrum showed a peak at 350 nm, which matches the absorption peak of NO_2^- (Figure S4C of the Supporting Information). Therefore, we conclude that NO_2^- is consumed during turnover. The product of the reaction involving NO_2^- could not be confirmed; however, oxidation of NO_2^- to NO_2 or NO_3^- at the OEC is very likely.

Enzyme Kinetics Probing the Mode of Inhibition of NO_2^- with Respect to Cl^-. O_2-evolution measurements were taken over a series of Cl^- and NO_2^- concentrations to identify the type of inhibition of NO_2^- with respect to Cl^- (Figure 3). The inhibition of PSII activity is multiphasic with respect to NO_2^- concentration (Figure 3), indicative of multiple sites of inhibition. Lineweaver−Burke plots, Dixon plots, and Cornish−Bowden plots were produced by considering Cl^- as the substrate and NO_2^- as the inhibitor (Figures 4−6). The essentially parallel lines for linear fits in the Lineweaver−Burke plot would normally suggest that NO_2^- is an uncompetitive inhibitor of PSII with respect to Cl^- (Figure 4). However, multiple modes of inhibition from NO_2^-, as observed by EPR (Figures 8 and 9, discussed below), may complicate the analysis. For a simple uncompetitive inhibition, the Dixon plot should also consist of parallel lines. The curvature of the points

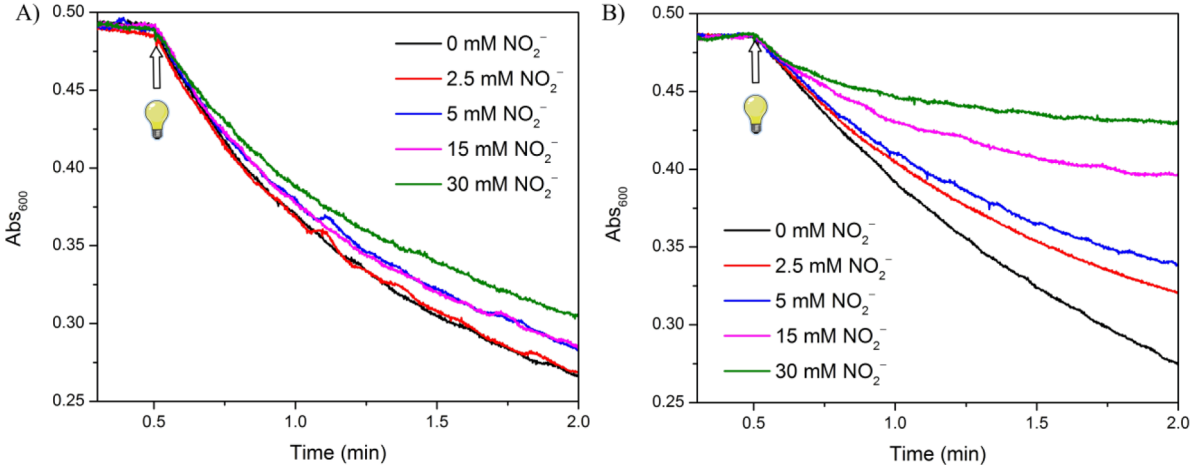

Figure 2. (A) DCPIP reduction assays using Mn-depleted, extrinsic polypeptide-depleted PSII membranes in the presence of different concentrations of NO_2^-, including DPC as a sacrificial source of electrons on the donor side. (B) DCPIP reduction assays using active PSII membranes in the presence of different concentrations of NO_2^-, using water as the source of electrons on the donor side under illumination.

dx.doi.org/10.1021/bi400206q | *Biochemistry* 2013, 52, 3781−3789

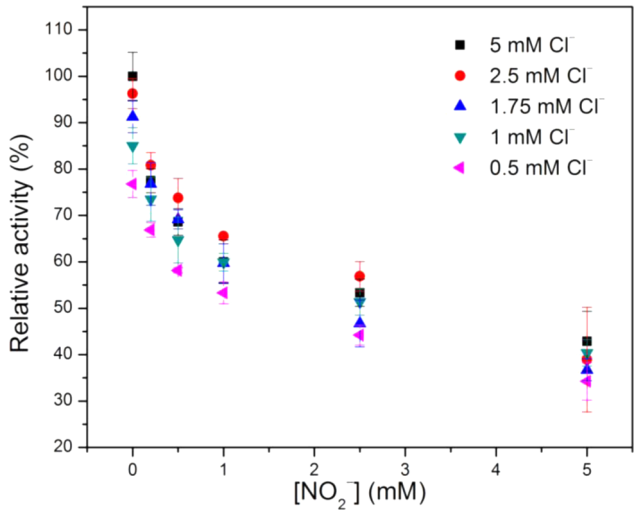

Figure 3. Relative activity (%) as a function of NO_2^- concentration in the presence of varying concentrations of Cl^-. The data points were normalized to the oxygen-evolution activity of each preparation in the presence of 10 mM Ca^{2+} and 5 mM Cl^- [these activities ranged from 400 to 530 μmol of O_2 (mg of Chl)$^{-1}$ h^{-1} and were set to 100%].

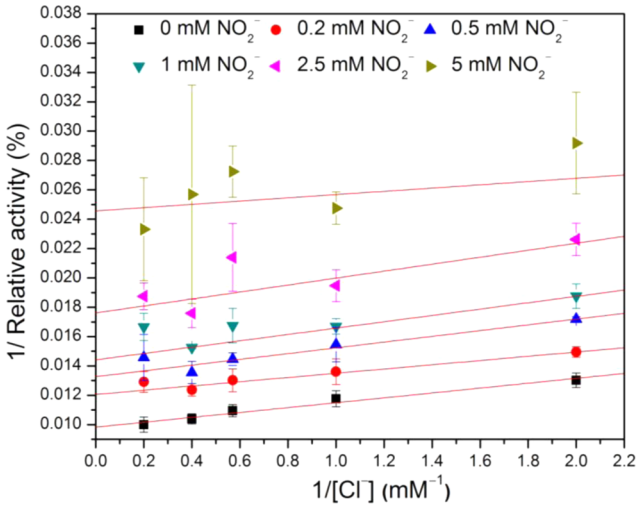

Figure 4. Lineweaver–Burke plot considering Cl^- as the substrate and NO_2^- as the inhibitor using the data set reported in Figure 3.

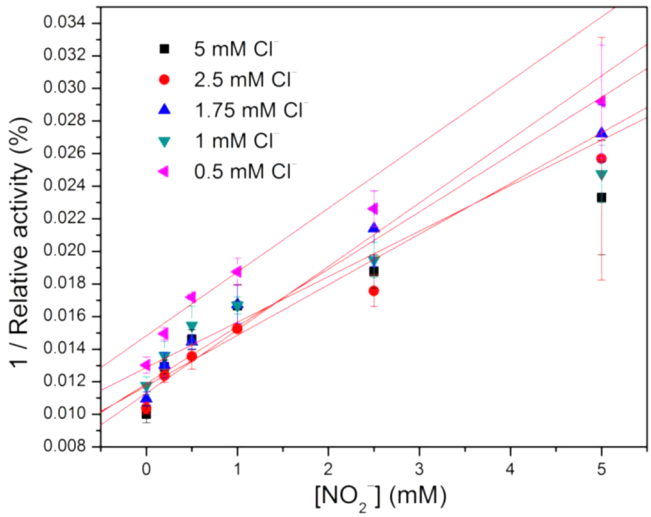

Figure 5. Dixon plot considering Cl^- as the substrate and NO_2^- as the inhibitor using the data set reported in Figure 3.

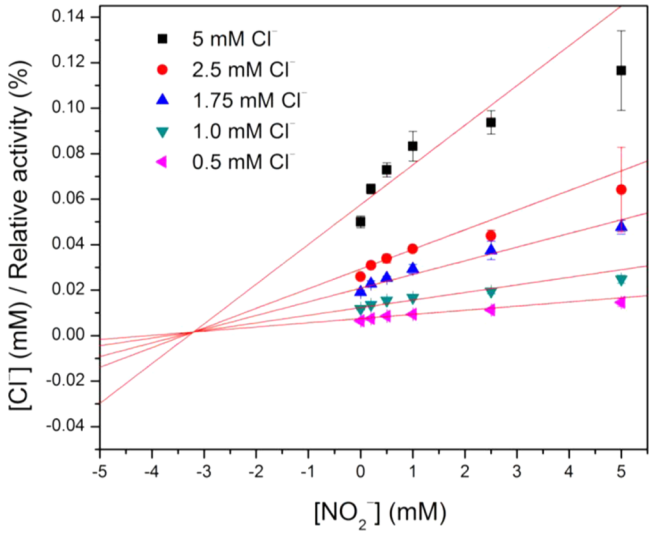

Figure 6. Cornish–Bowden plot considering Cl^- as the substrate and NO_2^- as the inhibitor using the data set reported in Figure 3.

in the Dixon plot suggests that there is a mixed-type inhibition, with more than one site for inhibition by NO_2^- (Figures 5 and 6). A similar Dixon plot has been reported for the inhibition from I^- with respect to Cl^-.[19] Furthermore, intersection of the linear fits at or below the *x*-axis in the Cornish–Bowden plot also indicates a noncompetitive or a mixed-type inhibition. A global fit of the Cornish–Bowden plot was achieved by constraining all linear fits to intersect at a single point, while both the intercepts and slopes were allowed to vary (Figure 6). The linear fits in the Cornish–Bowden plot intersect with an ordinate of $-K_I'$. As seen in Figure 3, the inhibition is multiphasic when the concentration of NO_2^- increases to 5 mM, with a more rapid decline in O_2 evolution for 0–0.5 mM NO_2^- than for higher NO_2^- concentrations of 1–5 mM. Separating the concentrations of NO_2^- above and below 0.5 mM and creating two separate Cornish–Bowden plots resulted in improved fits (Figure S5A,B of the Supporting Information), indicating at least two sites of inhibition where NO_2^- does not compete with Cl^-. The K_I's are approximately 1.3 and 7.5 mM for the two inhibitory sites, neither of which is the Cl^- site (Figure S5A,B of the Supporting Information). However, on the basis of the observation that NO_2^- is consumed during turnover (Figure S4C of the Supporting Information), it is also likely that a nonequilibrium concentration-dependent oxidation of NO_2^- occurs. Therefore, it is clear that NO_2^- inhibition of PSII is complicated and that a simple enzyme kinetics model is not sufficient to explain the results.

NO_2^- is an activator of PSII in Cl^--depleted PSII membranes,[16] which indicates that NO_2^- can occupy the Cl^--binding site in PSII. Although we were not able to determine a Cl^--competitive K_I from our enzyme kinetics analysis, our EPR data analysis, shown below (Figures 8 and 9), indicates competition between NO_2^- and Cl^- for the Cl^--binding site. It is possible that the K_I's for binding of NO_2^- to non-chloride sites in a mixed-type inhibition are much smaller than the K_I for the competition of NO_2^- with Cl^-, therefore resulting in a Lineweaver–Burke plot that does not show any competition of NO_2^- for the Cl^- site. Altogether, the steady-state O_2-evolution

dx.doi.org/10.1021/bi400206q | *Biochemistry* 2013, 52, 3781–3789

measurements are indicative of at least two non-chloride-binding sites for NO_2^- with K_I's that are smaller than the chloride-competitive K_I; the chloride-competitive K_I could not be determined from the steady-state enzyme kinetics analysis.

Flash-Induced Polarographic O_2 Measurements. Flash-induced polarographic O_2 yield measurements were taken with PSII membranes pelleted on a Pt disc/Ag ring electrode in the presence of 0, 2.5, 5, 15, and 30 mM NO_2^-. With increasing NO_2^- concentrations, the classic period-four oscillation pattern was perturbed and the yields of O_2 released during the flash sequence progression were dampened (Figure 7). The O_2

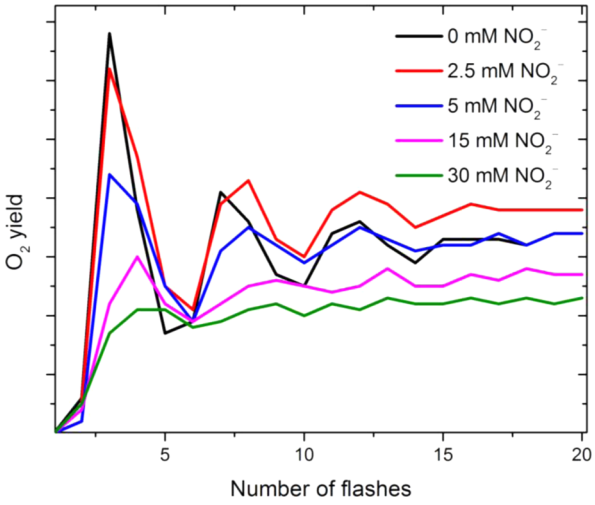

Figure 7. Flash-induced polarographic O_2 yield patterns for PSII membranes treated with different NO_2^- concentrations (labeled on the graph).

yields were fit using a four-S-state Kok model. The initial S_0- and S_1-state populations were obtained from the untreated sample (Table 1). To fit the data for samples with NO_2^-

Table 1. Percent Misses (α), Percent Double Hits (β), and S-State Distributions (percentages) of PSII Membranes Based on Fits Created Using a Four-State Kok Model[a]

$[NO_2^-]$ in assay buffer (mM)	α (% misses)	β (% double hits)	S_0 (%)	S_1 (%)
0	14.0	5.7	19.5	80.5
2.5	19.7	5.5	19.5[b]	80.5[b]
5	26.1	5.6	19.5[b]	80.5[b]
15	44.3	6.8	19.5[b]	80.5[b]

[a]The initial S_0- and S_1-state populations were obtained by fitting the data for the untreated sample (0 mM sample). [b]For samples treated with NO_2^-, the initial S_0- and S_1-state populations were fixed to the values obtained for an untreated sample.

present, the double hits and misses were allowed to change while the initial S_0- and S_1-state populations were restricted to 19.5 and 80.5%, respectively, as found in the untreated sample (Table 1). The percent of double hits remained fairly constant, whereas the percent misses drastically increased with increasing NO_2^- concentrations (Table 1). Reduction of the OEC by NO_2^- in the time between flashes in the flash-induced polarographic O_2 measurements is revealed by the increase in misses. This is consistent with NO_2^- oxidation by the OEC during turnover (Figure S4 of the Supporting Information).

The redox chemistry of NO_2^- with the OEC is an attractive suggestion for its inhibitory effect on the donor side. A parallel study conducted to probe the chemistry of NO_2^- with di-μ-oxodimanganese complexes shows that Mn(III/IV) dimers oxidize NO_2^- to NO_3^- (Y. Gao, R. Pokhrel, and G. W. Brudvig, manuscript in preparation). It was found that NO_2^- can bind to Mn in the model complex in place of a water molecule and undergo a two-electron oxidation. Analogously, we propose that NO_2^- can bind in place of one or more of the terminal water molecules in the OEC and undergo a two-electron oxidation. Our EPR analysis shows that the S_1 state is not reduced by NO_2^- because the yield of the S_2-state signal under single-turnover conditions is not changed by a 2 h incubation of the sample with NO_2^- in the dark (Figure 8), as discussed in the following section. Therefore, the oxidation of NO_2^- is most likely occurring in the higher S states, such as the S_2 and/or S_3 states of the OEC.

EPR Spectroscopy. *Donor Side.* EPR experiments show that the total yield of the S_2 state remained unchanged in the presence of up to 15 mM NO_2^- (Figure 8A). These results indicate that the significant inhibition observed in the O_2-evolution measurements up to 5 mM NO_2^- occurred during turnover in one or more of the S states higher than the S_1 state, possibly the S_2 and S_3 states, in agreement with previous studies[16] and flash-induced polarographic O_2 yield measurements. At higher NO_2^- concentrations, 30 and 60 mM, the total yield of the S_2 state, the sum of the $g = 4.1$ and $g = 2$ multiline signals, decreased. However, increasing concentrations of NO_2^- stabilized the $g = 4.1$ form over the $g = 2$ multiline form (Figures 8 and 9). Substitution of Cl^- with NO_2^- at high NO_2^- concentrations could cause a shift in the equilibrium toward the $g = 4.1$ state, consistent with a similar effect for the substitution of Cl^- with other monovalent anions and primary amines.[17,28−31]

Acceptor Side. Earlier studies demonstrated that several anions bind to the non-heme Fe(II) on the acceptor side of PSII[4,8,32,33] and that their binding slows or completely blocks electron transfer on the acceptor side.[8,33] NO_2^- was shown to bind reversibly to a site where it can be displaced by bicarbonate,[8,33] and it can be concluded that NO_2^- binds to the non-heme Fe(II) in PSII, consistent with our findings. It was also found that the K_d of $H^{14}CO_3^-$ of 81 μM was increased to 238 μM by the addition of 5 mM NO_2^- and increased to 481 μM by the addition of 10 mM NO_2^-, indicating competitive binding.[22] Furthermore, NO_2^- showed stronger inhibition of HCO_3^- binding under illumination than in the dark.[22] In the presence of 2 mM $NaNO_2$, the K_d of HCO_3^- was 171 μM in the dark and increased to 706 μM after illumination under room light for 30 min.[22] Therefore, NO_2^- is a more powerful competitor for the HCO_3^--binding site under illumination. Variable fluorescence studies showed that the $t_{1/2}$ for the $Q_A^-Q_B \rightarrow Q_AQ_B^-$ reaction is increased from 0.8 to 4.0 ms in the presence of 20 mM NO_2^-.[34] However, our UV−visible studies show that there is no significant change in the rate of DCPIP reduction in Mn-depleted PSII membranes at ≤30 mM NO_2^-.

In the light-minus-dark EPR spectrum of PSII samples without any NO_2^- in this study, a $g = 1.9$ Fe(II)-$Q_A^{-\bullet}$ signal from the acceptor side was observed (Figure 8). However, in the presence of NO_2^-, a broad $g = 1.6$ signal and another $g = 7$ feature also appeared in the light-minus-dark spectra (Figure 8). The yield of the broad $g = 1.6$ signal and the $g = 7$ signal remained unchanged with the NO_2^- concentration increasing

dx.doi.org/10.1021/bi400206q | Biochemistry 2013, 52, 3781−3789

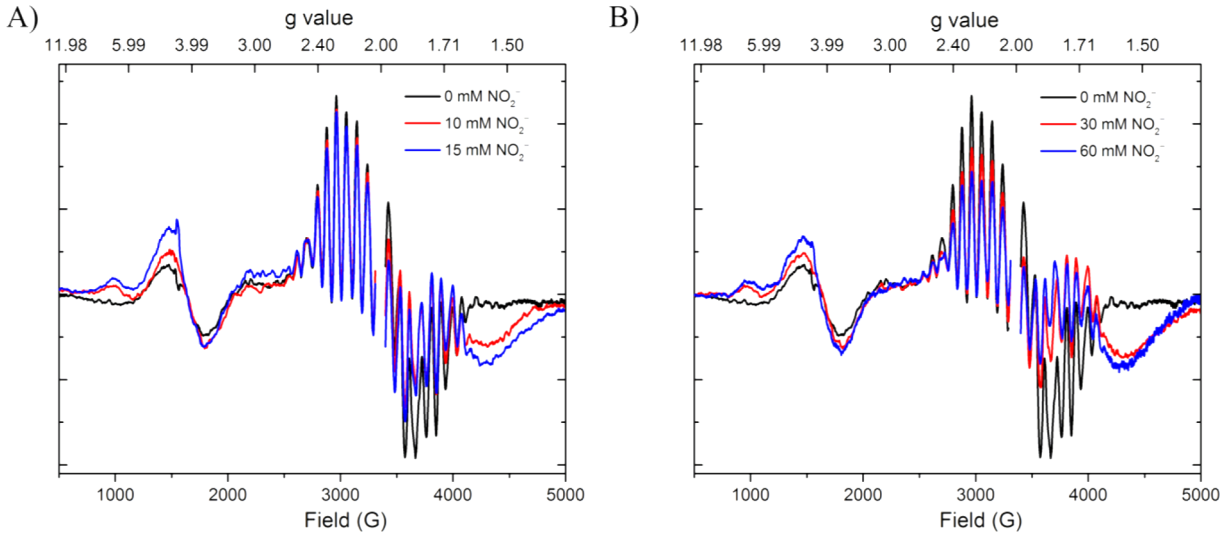

Figure 8. (A) Light-minus-dark EPR spectra with 0, 10, and 15 mM NO_2^-. (B) Light-minus-dark EPR spectra with 0, 30, and 60 mM NO_2^-. All EPR samples of PSII membranes were advanced to the S_2 state by illumination in a 200 K dry ice/acetone bath for 5 min.

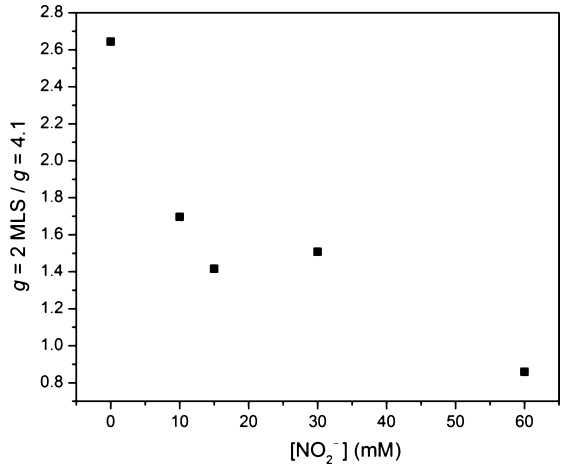

Figure 9. Ratio of the g = 2 multiline signal (MLS) and the g = 4.1 signal as a function of NO_2^- concentration.

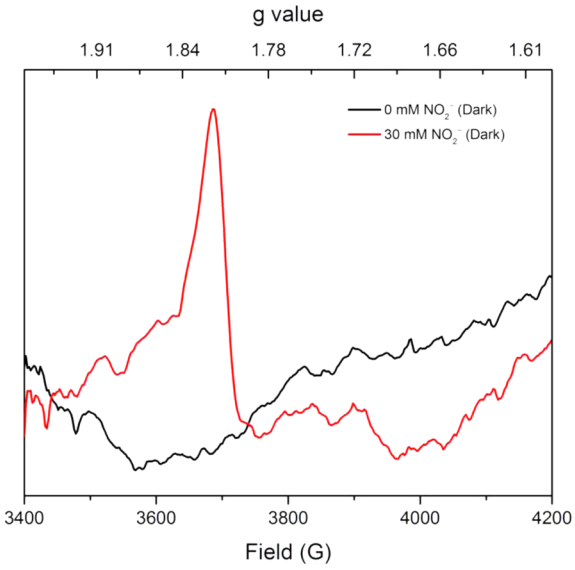

Figure 10. Dark EPR spectra of PSII membrane samples prepared in the absence of NO_2^- (black) and in the presence of 30 mM NO_2^- (red). Spectra were collected at 4 K with a microwave power of 20 mW.

from 15 to 60 mM. These signals are tentatively assigned to arise from a NO_2^--bound Fe(II)-$Q_A^{-\bullet}$ species. A similar difference spectrum has also been observed in samples that were initially treated with NO, which was then removed from the sample.[35]

In the presence of NO_2^-, a g = 1.8 signal appeared in the dark EPR spectrum that was not present in its absence (Figure 10). This signal resembled the well-characterized Fe(II)-$Q_A^{-\bullet}$ signal observed in certain carboxylate-bound Fe(II)-$Q_A^{-\bullet}$ species and bicarbonate-depleted Fe(II)-$Q_A^{-\bullet}$.[8,36−38] The presence of this signal demonstrates the coordination of the non-heme iron by Fe(II) by NO_2^-, and either the reduction of Q_A or the reduction of Q_B. EPR results clearly showed that the S_1- to S_2-state transition was not blocked at ≤15 mM NO_2^- (Figure 8A), which indicates that Q_A was not reduced in the dark at these NO_2^- concentrations. If Q_A was reduced in the dark, it would prevent a stable charge separation upon illumination, and the S state of the OEC would not be advanced. Therefore, the g = 1.8 dark signal arises from a NO_2^--bound Fe(II)-$Q_B^{-\bullet}$ species, and not from a NO_2^--bound Fe(II)-$Q_A^{-\bullet}$ species.

The intensity of the NO_2^--bound Fe(II)-$Q_B^{-\bullet}$ g = 1.8 dark signal decreased with an increasing concentration of NO_2^- (Figure 11), indicating that Q_B becomes either doubly reduced or reoxidized at higher NO_2^- concentrations. However, because the E^0 value for one-electron oxidation of NO_2^- is approximately −0.99 V, it is not feasible for it to directly reduce Q_B to $Q_B^{-\bullet}$. Therefore, alternative schemes are proposed for the reduction of Q_B, in which the non-heme Fe is involved. The standard potentials at pH 6 for oxidation and reduction of NO_2^- are listed below.

$$NO_2^- + 2H^+ + e^- \rightarrow NO + H_2O \; E^0 = 0.47 \text{ V}$$

$$NO_2^- + H_2O \rightarrow NO_3^- + 2H^+ + 2e^- \; E^0 = -0.47 \text{ V}$$

$$NO_2^- \rightarrow NO_2 + e^- \; E^0 = -0.99 \text{ V}$$

dx.doi.org/10.1021/bi400206q | Biochemistry 2013, 52, 3781−3789

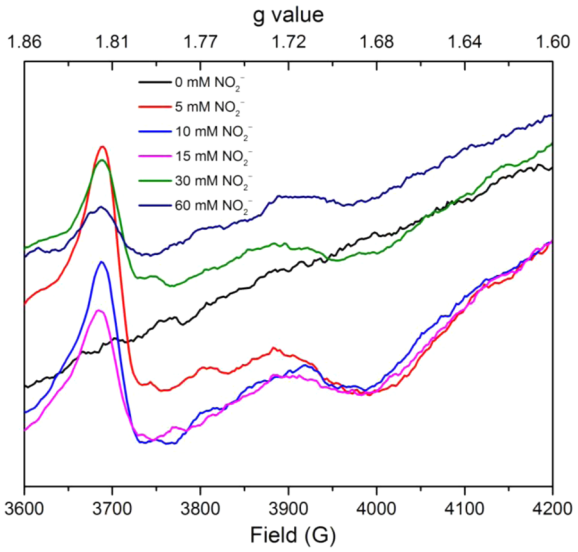

Figure 11. Dark EPR spectra of PSII membrane samples prepared in the presence of 0, 5, 10, 15, 30, and 60 mM NO_2^-. Spectra were collected at 7 K with a microwave power of 5 mW.

Because the Q_B to $Q_B^{-\bullet}$ reduction is a one-electron reduction and the only feasible oxidation of NO_2^- is a two-electron oxidation of NO_2^- to NO_3^-, we propose a non-heme Fe(II)-catalyzed reduction of Q_B. The midpoint redox potential of the non-heme Fe(II) is estimated to be approximately 400 mV.[39] Initially, NO_2^- bound to the non-heme Fe(II) could oxidize the non-heme Fe(II) to Fe(III), resulting in the production of NO. Because NO reacts with O_2 under aerobic conditions and because NO_2^- is present in excess, NO formed at the non-heme iron site would subsequently be replaced by a second equivalent of NO_2^-. NO_2^- bound to Fe(III) can undergo a two-electron oxidation to NO_3^-, where one electron is used to reduce Fe(III) to Fe(II) and the other electron is used to reduce Q_B to $Q_B^{-\bullet}$. Once again, because NO_2^- is present in excess, NO_2^- would displace the NO_3^- bound to the non-heme Fe(II) site. However, the reoxidation of $Q_B^{-\bullet}$ to Q_B is also feasible via the reduction of NO_2^- to NO. This could explain the observation that the magnitude of the $g = 1.8$ Fe(II)-$Q_B^{-\bullet}$ signal generated in the dark at low concentrations of NO_2^- decreases as the concentration of NO_2^- is increased (Figure 11).

The light-induced S_2-minus-S_1 difference spectra for NO_2^--treated PSII show a broad $g = 1.6$ feature in place of the $g = 1.9$ Fe(II)-$Q_A^{-\bullet}$ signal present in untreated samples. We propose that the broad signal arises from a NO_2^--bound Fe(II)-$Q_A^{-\bullet}$ species. However, the reason for the significant difference in the EPR signals for the dark NO_2^--bound Fe(II)-$Q_B^{-\bullet}$ species and the light-induced NO_2^--bound Fe(II)-$Q_A^{-\bullet}$ species is not obvious.

Reversibility of NO_2^- Effects. PSII membranes that had been previously treated with 60 mM NO_2^- were tested for the ability to recover the EPR signals generated in untreated PSII samples: the S_2-state $g = 2$ multiline signal, the S_2-state $g = 4.1$ signal, and the $g = 1.9$ Fe^{2+}-$Q_A^{-\bullet}$ signal. Following 200 K illumination to yield the S_2-state EPR spectrum in the presence of 60 mM NO_2^-, the sample was thawed on ice, washed with NO_2^--free buffer in the dark, and incubated in the dark for 30 min. The "washed" sample gave almost identical yields of the $g = 2$ multiline, $g = 4.1$, and $g = 1.9$ Fe^{2+}-$Q_A^{-\bullet}$ signals compared to those of the untreated sample (Figure S6 of the Supporting Information). The broad $g = 1.6$ signal also disappeared upon washing (Figure S6 of the Supporting Information). Because of the restored yield of the S_2 state, we can conclude that the OEC was intact throughout our experiments and was not reduced by treating PSII membranes with up to 60 mM NO_2^-. The lower yield of the $g = 2$ multiline signal and the $g = 4.1$ signal in the presence of $\geq$ 30 mM NO_2^- may have been due to either another form of the S_2 state of the OEC that is not observed under these conditions or a less efficient charge separation at these NO_2^- concentrations, as indicated by the lower yield of the $S_1Y_Z^{\bullet}$ state in the 60 mM NO_2^--treated PSII membranes when compared to the untreated PSII membranes (Figure S7 of the Supporting Information).

CONCLUSIONS

In this work, we investigated the binding and chemistry of NO_2^- with PSII. A previous study had shown that NO_2^- can bind in place of Cl^- in Cl^--depleted PSII membranes.[16] Using steady-state O_2-evolution assays, we investigated the competition between NO_2^- and Cl^- for the Cl^--binding site in PSII membranes that were not depleted of Cl^-. At $\leq$5 mM NO_2^-, we observed mixed-type inhibition by NO_2^-. Two K_I's for NO_2^- inhibition were estimated to be around 1.3 and 7.5 mM. These two non-chloride sites for NO_2^- inhibition are proposed to be the non-heme Fe site and the OEC. The Cl^--competitive K_I, estimated from EPR measurements to be much higher than the K_I's of the non-chloride sites, could not be determined from the steady-state activity assays. Electron-transfer assays confirmed that the inhibition was largely a donor side effect. UV−visible spectroscopy showed that NO_2^- was consumed during turnover. Flash-induced polarographic O_2 yield measurements confirmed an increase in the miss parameter with an increasing NO_2^- concentration. Therefore, we propose that NO_2^- is oxidized by the OEC in one or more of the S states above S_1, resulting in reduction of the OEC. A separate investigation of the reaction of NO_2^- with di-μ-oxodimanganese complexes showed that Mn(III/IV) dimers oxidize NO_2^- to NO_3^- (Y. Gao, R. Pokhrel, and G. W. Brudvig, manuscript in preparation), consistent with our proposal for the oxidation of NO_2^- by the OEC.

In our EPR experiments, the $S_1 \rightarrow S_2$ transition proceeded in full yield in the presence of $\leq$15 mM NO_2^-. At 30 and 60 mM NO_2^-, a decrease in the yield of the S_2 EPR signals was observed, although the magnitude of the $g = 4.1$ form of the S_2 state increased relative to the magnitude of the $g = 2$ multiline signal. This observation is consistent with the competition of NO_2^- for the Cl^- site in the higher NO_2^- concentration regime, because depletion or substitution of Cl^- with other monovalent anions has been shown to favor the $g = 4.1$ form of the S_2 state. Additionally, in the presence of NO_2^-, the $g = 1.9$ Fe(II)-$Q_A^{-\bullet}$ signal was replaced by a broad $g = 1.6$ signal, and NO_2^- reduced Q_B in the dark, giving rise to a $g = 1.8$ signal that was assigned to NO_2^--bound Fe(II)-$Q_B^{-\bullet}$.

ASSOCIATED CONTENT

Supporting Information

Additional activity assay data on the effect of incubation time, concentration, and acceptor side effects of NO_2^-; pH dependence of oxygen-evolution activity in the presence and absence of chloride; UV−visible spectra showing NO_2^- consumption; additional Cornish−Bowden plots; and additional EPR spectra on the effect of NO_2^- on the S_2 state and

dx.doi.org/10.1021/bi400206q | Biochemistry 2013, 52, 3781−3789

$S_1Y_Z^•$ signals. This material is available free of charge via the Internet at http://pubs.acs.org.

AUTHOR INFORMATION

Corresponding Author

*E-mail: gary.brudvig@yale.edu. Phone: (203) 432-5202. Fax: (203) 432-6144.

Funding

This work was supported by Grant DE-FG02-05ER15646 from the Department of Energy, Office of Basic Energy Sciences, Division of Chemical Sciences.

Notes

The authors declare no competing financial interest.

ABBREVIATIONS

Chl, chlorophyll; DCBQ, 2,5-dichlorobenzoquinone; DCPIP, 2,6-dichlorophenolindophenol; DPC, diphenyl carbazide; EPR, electron paramagnetic resonance; EXAFS, extended X-ray absorption fine structure; MES, 2-(*N*-morpholino)-ethanesulfonic acid; OEC, oxygen-evolving complex; PSII, photosystem II; Y_Z, D1-tyrosine 161.

REFERENCES

(1) Umena, Y., Kawakami, K., Shen, J.-R., and Kamiya, N. (2011) Crystal structure of oxygen-evolving photosystem II at a resolution of 1.9 Å. *Nature 473*, 55−60.

(2) McEvoy, J. P., and Brudvig, G. W. (2004) Structure-based mechanism of photosynthetic water oxidation. *Phys. Chem. Chem. Phys. 6*, 4754−4763.

(3) Kok, B., Forbush, B., and McGloin, M. (1970) Cooperation of charges in photosynthetic oxygen evolution. I. A linear four step mechanism. *Photochem. Photobiol. 11*, 457−475.

(4) Diner, B. A., and Petrouleas, V. (1990) Formation by nitric oxide of nitrosyl adducts of redox components of the photosystem II reaction center. II. Evidence that bicarbonate/carbon dioxide binds to the acceptor-side non-heme iron. *Biochim. Biophys. Acta 1015*, 141−149.

(5) Cox, N., Jin, L., Jaszewski, A., Smith, P. J., Krausz, E., Rutherford, A. W., and Pace, R. (2009) The semiquinone-iron complex of photosystem II: Structural insights from ESR and theoretical simulation; evidence that the native ligand to the non-heme iron is carbonate. *Biophys. J. 97*, 2024−2033.

(6) Chernev, P., Zaharieva, I., Dau, H., and Haumann, M. (2011) Carboxylate shifts steer interquinone electron transfer in photosynthesis. *J. Biol. Chem. 286*, 5368−5374.

(7) Hermes, S., Bremm, O., Garczarek, F., Derrien, V., Liebisch, P., Loja, P., Sebban, P., Gerwert, K., and Haumann, M. (2006) A time-resolved iron-specific X-ray absorption experiment yields no evidence for an $Fe^{2+} \rightarrow Fe^{3+}$ transition during $Q_A^- \rightarrow Q_B$ electron transfer in the photosynthetic reaction center. *Biochemistry 45*, 353−359.

(8) Petrouleas, V., Deligiannakis, Y., and Diner, B. A. (1994) Binding of carboxylate anions at the non-heme Fe(II) of PS II. II. Competition with bicarbonate and effects on the Q_A/Q_B electron transfer rat. *Biochim. Biophys. Acta 1188*, 271−277.

(9) Pokhrel, R., McConnell, I. L., and Brudvig, G. W. (2011) Chloride regulation of enzyme turnover: Application to the role of chloride in photosystem II. *Biochemistry 50*, 2725−2734.

(10) Critchley, C. (1985) The role of chloride in photosystem II. *Biochim. Biophys. Acta 811*, 33−46.

(11) Lindberg, K., Vänngård, T., and Andréasson, L. E. (1993) Studies of the slowly exchanging chloride in photosystem II of higher plants. *Photosynth. Res. 38*, 401−408.

(12) Murray, J. W., Maghlaoui, K., Joanna, K., Naoko, I., Lai, T.-L., Rutherford, A. W., Sugiura, M., Boussac, A., and Barber, J. (2008) X-ray crystallography identifies two chloride binding sites in the oxygen evolving centre of Photosystem II. *Energy Environ. Sci. 1*, 161−166.

(13) Kawakami, K., Umena, Y., Kamiya, N., and Shen, J. R. (2009) Location of chloride and its possible functions in oxygen-evolving photosystem II revealed by X-ray crystallography. *Proc. Natl. Acad. Sci. U.S.A. 106*, 8567−8572.

(14) Guskov, A., Kern, J., Gabdulkhakov, A., Broser, M., Zouni, A., and Saenger, W. (2009) Cyanobacterial photosystem II at 2.9 Å resolution and the role of quinones, lipids, channels and chlorid. *Nat. Struct. Mol. Biol. 16*, 334−342.

(15) Haumann, M., Barra, M., Loja, P., Loescher, S., Krivanek, R., Grundmeier, A., Andréasson, L.-E., and Dau, H. (2006) Bromide does not bind to the Mn_4Ca complex in its S_1 state in Cl^--depleted and Br^--reconstituted oxygen-evolving photosystem II: Evidence from X-ray absorption spectroscopy at the Br K-edge. *Biochemistry 45*, 13101−13107.

(16) Wincencjusz, H., Yocum, C. F., and van Gorkom, H. J. (1999) Activating anions that replace Cl^- in the O_2-evolving complex of photosystem II slow the kinetics of the terminal step in water oxidation and destabilize the S_2 and S_3 states. *Biochemistry 38*, 3719−3725.

(17) Kühne, H., Szalai, V. A., and Brudvig, G. W. (1999) Competitive binding of acetate and chloride in photosystem II. *Biochemistry 38*, 6604−6613.

(18) Haddy, A., Hatchell, J. A., Kimel, R. A., and Thomas, R. (1999) Azide as a competitor of chloride in oxygen evolution by Photosystem II. *Biochemistry 38*, 6104−6110.

(19) Bryson, D. I., Doctor, N., Johnson, R., Baranov, S., and Haddy, A. (2005) Characteristics of iodide activation and inhibition of oxygen evolution by photosystem II. *Biochemistry 44*, 7354−7360.

(20) Hasegawa, K., Kimura, Y., and Ono, T. A. (2002) Chloride cofactor in the photosynthetic oxygen-evolving complex studied by Fourier transform infrared spectroscopy. *Biochemistry 41*, 13839−13850.

(21) Wincencjusz, H., Yocum, C. F., and van Gorkom, H. J. (1998) S-state dependence of chloride binding affinities and exchange dynamics in the intact and polypeptide-depleted O_2 evolving complex of photosystem II. *Biochemistry 37*, 8595−8604.

(22) Stemler, A. J., and Murphy, J. B. (1985) Bicarbonate-reversible and irreversible inhibition of PS II by monovalent anions. *Plant Physiol. 77*, 974−977.

(23) Sinclair, J. (1987) Changes in spinach thylakoid activity due to nitrite ions. *Photosynth. Res. 12*, 255−263.

(24) Sahay, A., Jajoo, A., and Bharti, S. (2006) A thermoluminescence study of the effects of nitrite on photosystem II in spinach thylakoids. *Luminescence 21*, 143−147.

(25) Berthold, D. A., Babcock, G. T., and Yocum, C. F. (1981) A highly resolved, oxygen-evolving photosystem II preparation from spinach thylakoid membranes. EPR and electron-transport properties. *FEBS Lett. 134*, 231−234.

(26) Miyao, M., and Inoue, Y. (1991) Enhancement by chloride ions of photoactivation of oxygen evolution in manganese-depleted photosystem II membranes. *Biochemistry 30*, 5379−5387.

(27) Miyao, M., and Inoue, Y. (1991) An improved procedure for photoactivation of photosynthetic oxygen evolution: Effect of artificial electron acceptors on the photoactivation yield of hydroxylamine-treated wheat photosystem II membranes. *Biochim. Biophys. Acta 1056*, 47−56.

(28) Olesen, K., and Andréasson, L. E. (2003) The function of the chloride ion in photosynthetic oxygen evolution. *Biochemistry 42*, 2025−2035.

(29) Ono, T., Nakayama, H., Gleiter, H., Inoue, Y., and Kawamori, A. (1987) Modification of the properties of S_2 state in photosynthetic oxygen-evolving center by replacement of chloride with other anions. *Arch. Biochem. Biophys. 256*, 618−624.

(30) Beck, W. F., and Brudvig, G. W. (1986) Binding of amines to the O_2-evolving center of photosystem II. *Biochemistry 25*, 6479−6486.

(31) Haddy, A., Kimel, R. A., and Thomas, R. (2000) Effects of azide on the S_2 state EPR signals from photosystem II. *Photosynth. Res. 63*, 35−45.

(32) Deligiannakis, Y., Petrouleas, V., and Diner, B. A. (1994) Binding of carboxylate anions at the non-heme Fe(II) of PS II. I. Effects on the Q_AFe^{2+} and Q_AFe^{3+} EPR spectra and the redox properties of the iron. *Biochim. Biophys. Acta 1188*, 260−270.
(33) Koulougliotis, D., Kostopoulos, T., Petrouleas, V., and Diner, B. A. (1993) Evidence for CN-binding at the photosystem II non-heme Fe^{2+}. Effects on the EPR signal for Q_AFe^{2+} and on Q_A/Q_B electron transfer. *Biochim. Biophys. Acta 1141*, 275−282.
(34) Jursinic, P., and Stemler, A. (1988) Multiple anion effects on photosystem II in chloroplast membranes. *Photosynth. Res. 15*, 41−56.
(35) Ioannidis, N., Sarrou, J., Schansker, G., and Petrouleas, V. (1998) NO reversibly reduces the water-oxidizing complex of photosystem II through S_0 and S_{-1} to the state characterized by the Mn(II)-Mn(III) multiline EPR signal. *Biochemistry 37*, 16445−16451.
(36) Rutherford, A. W., and Zimmermann, J. L. (1984) A new EPR signal attributed to the primary plastosemiquinone acceptor in photosystem II. *Biochim. Biophys. Acta 767*, 168−175.
(37) Vermaas, W. F. J., and Rutherford, A. W. (1984) EPR measurements on the effects of bicarbonate and triazine resistance on the acceptor side of photosystem II. *FEBS Lett. 175*, 243−248.
(38) Hallahan, B. J., Ruffle, S. V., Bowden, S. J., and Nugent, J. H. A. (1991) Identification and characterization of EPR signals involving Q_B semiquinone in plant photosystem II. *Biochim. Biophys. Acta 1059*, 181−188.
(39) Diner, B. A., and Petrouleas, V. (1987) Q400, the non-heme iron of the photosystem II iron-quinone complex. A spectroscopic probe of quinone and inhibitor binding to the reaction center. *Biochim. Biophys. Acta 895*, 107−125.